THE JOURNAL OF PHYSICAL CHEMISTRY B

Article

pubs.acs.org/JPCB

Hydrogen Bonding Induced Enhancement of Fermi Resonances: Ultrafast Vibrational Energy Flow Dynamics in Aniline-d_5

Rene Costard, Christian Greve, Henk Fidder, and Erik T. J. Nibbering*

Max Born Institut für Nichtlineare Optik und Kurzzeitspektroskopie, , Max Born Strasse 2A, D-12489 Berlin, Germany

Supporting Information

ABSTRACT: With hydrogen bonding of the amino group of aniline-d_5 we can identify the roles of Fermi enhanced combination and overtone states in intramolecular vibrational re-distribution (IVR) pathways for N−H stretching excitations. Using linear Fourier transform infrared (FT-IR) spectroscopy, ultrafast one- and two-color IR-pump−IR-probe spectroscopy, and femtosecond two-dimensional IR spectroscopy, we can identify the primary accepting modes for N−H stretching excitations. In particular, a key role is played by the $\delta(NH_2)$ bending degree of freedom, either via its $\delta = 2$ overtone state or via a combination state with the ν(C═C) ring stretching mode. No significant transient population in these Fermi enhanced combination/overtone states can be observed, a consequence of similar decay rates of these Fermi enhanced combination/overtone states and of the N−H stretching states. A similar magnitude of the transient response of the two fingerprint modes regardless of direct excitation of the Fermi enhanced combination/overtone levels or of the N−H stretching states suggests an underlying coupling mechanism facilitating common IVR pathways. This mechanism is expected to be of general importance for other organic compounds with hydrogen-bonded amino groups, including DNA bases.

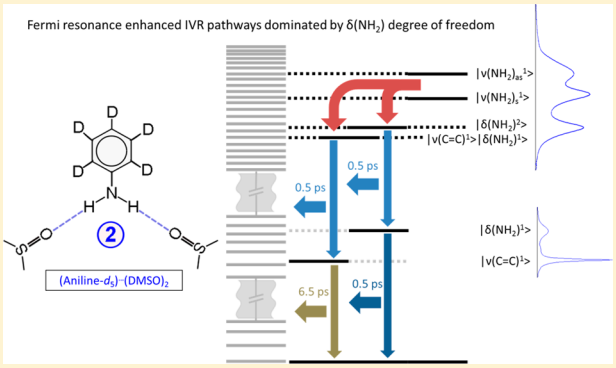

INTRODUCTION

Fermi resonances play an important role in vibrational spectra of molecules. Quantum mechanical mixing of vibrational states, typically between a fundamental and an overtone state, leads to a linear combination of these states with altered frequencies and an associated re-distribution of the oscillator strengths.[1] As a result, formally forbidden overtone transitions borrow oscillator strength from the mixed-in optically allowed fundamental transition, leading to significant cross-sections. The prominence of these features depends critically on the coupling strength and the energy gap between the mixed states. The latter can be influenced by chemical interactions, such as hydrogen bonding, where the magnitude of hydrogen bonding is reflected in the transfer of hydrogen stretching oscillator strength to Fermi enhanced overtones of hydrogen bending modes.[2−6] Numerous cases have been reported where the description of the O−H or N−H stretching line shapes are rather involved. For these medium strong hydrogen-bonded examples the O−H/N−H stretching modes exhibit not only Fermi resonances with several overtone/combination states of fingerprint modes but also even low-frequency mode progressions due to anharmonic couplings with hydrogen-bond deformation modes, which make their vibrational spectroscopy a rich topic.[7−21] Such a detailed determination of vibrational structure of N−H/O−H stretching modes provides a profound insight into the underlying vibrational couplings to be used as input for advanced quantum chemical calculations of the microscopic structure of hydrogen-bonded systems, including acid−base pairs.[22] Recently we reported on the effect of hydrogen bonding between aniline-d_5 and dimethyl sulfoxide[23] on the N−H stretching manifold of aniline-d_5, which is also an excellent model system for the effect of hydrogen bonding on DNA bases.[24] We demonstrated that the observed spectral changes are quantitatively captured by including a dominant Fermi resonance between the N−H stretching modes and the NH_2 bending mode overtone. Here the N−H stretching degrees of freedom of the amino group are in strong interaction with the NH_2 bending mode, enabling a proper description of the linear and two-dimensional infrared (2D-IR) spectroscopy of the fundamental and first overtone states of the N−H stretching manifolds using a simple hybrid Hamiltonian consisting of the NH_2 bending and the two local N−H stretching degrees of freedom.

Fermi resonances not only alter the quantum chemical nature of vibrationally excited states but also strongly influence the vibrational energy flow pathways through which molecular systems ultimately re-distribute the vibrational excitations en-route to dissipation channels involving the surrounding

Special Issue: Photoinduced Proton Transfer in Chemistry and Biology Symposium

Received: October 2, 2014
Revised: November 12, 2014
Published: November 13, 2014

   dx.doi.org/10.1021/jp509977r | J. Phys. Chem. B 2015, 119, 2711−2725

solvent.[25−30] Typically, for medium-sized molecules in the condensed phase intramolecular vibrational re-distribution (IVR) occurs on (sub)picosecond time scales, whereas vibrational energy relaxation (VER) by dissipation to the solvent takes place on time scales ranging from a few to a few tens of picoseconds.[31,32] For hydrogen stretching oscillators it has been argued that the primary relaxation route for the $\nu = 1$ state of the hydrogen stretching mode is facilitated by the bending overtone $\delta = 2$ state. The Fermi resonance facilitates an IVR pathway with the bending mode acting as the primary accepting mode of the hydrogen stretching excitation, followed by subsequent vibrational re-distribution in secondary accepting modes de-exciting the bending degree of freedom. In fact, more than 35 years ago Kaiser and co-workers have explained picosecond IR-pump/anti-Stokes-Raman-probe spectroscopic results on organic molecules such as benzene or toluene,[33] and $CHCl_3$ or CH_3I[34] by arguing that C−H stretching excitations re-distribute via C−H bending overtone states. Dlott and co-workers have shown that re-distribution scenarios of C−H stretching excitations in polyatomic molecules do not exclusively lead to a transient population of C−H bending modes, as other fingerprint modes can play a decisive role as well.[35] Using the same technique a similar conclusion has been drawn for O−H- and N−H stretching excitations of medium strong hydrogen-bonded systems, for which the O−H- and N−H stretching manifolds reflect the multitude of Fermi resonances and anharmonic couplings with low-frequency modes.[36−38] In contrast, water has only three vibrational internal degrees of freedom. From gas phase studies the Fermi resonance effect between the fundamental $\nu = 1$ O−H stretching and first overtone $\delta = 2$ H_2O bending states is understood to be large,[6,39−41] as opposed to the corresponding states of HOD, where the energy mismatch is much larger. Femtosecond IR-pump−IR-probe experiments on bulk water and on confined water have shown that this Fermi resonance facilitates an efficient IVR route transiently populating the bend fundamental $\delta = 1$ state, before the vibrational energy is re-distributed further into intermolecular librational and hydrogen bond translational degrees of freedom.[42−44] For isotopically diluted water under ambient conditions (i.e., HOD in H_2O or in D_2O), the energy mismatch between the stretching fundamental and bending first overtone states is too large to facilitate an efficient ultrafast IVR pathway as in neat liquid water.[45] In a recent study by Schäfer et al., it has been found that the frequency upshift of the fundamentally excited-state of the O−D stretching mode in HOD in supercritical water results in a Fermi resonance enhancement with the bending first overtone, as probed by femtosecond IR-pump−IR-probe spectroscopy.[46]

An experimental demonstration of a vibrational cascade within the hydrogen stretching manifold has not yet been reported; i.e., a sequential kinetics scheme, that upon $\nu = 0 \rightarrow \nu = 1$ hydrogen stretching excitation population transfer to the $\delta = 2$ overtone bending state occurs, before further re-distribution to the $\delta = 1$ fundamental bending state or other states takes place. C−H stretching $\nu = 1$ states may be involved in Fermi resonances with C−H bending overtone states, but typical relaxation dynamics of C−H $\nu = 1$ stretching states on picosecond time scales prevents an unequivocal detection of transient population buildup of the C−H bending $\delta = 2$ overtone states.[47,48] This also holds for O−H or N−H v=1 stretching states of non-hydrogen-bonded systems. However, not only does hydrogen bonding lead to a profound frequency downshift of the O−H- or N−H stretching vibration, causing a stronger Fermi resonance effect with the bending overtone, but also a lifetime shortening of the hydrogen stretching oscillator may facilitate an experimental probing of the suggested IVR mechanism. Line broadening of O−H stretching bands of condensed phase hydrogen-bonded molecular systems such as H_2O typically prevents a clear distinction between O−H stretching and bending overtone transitions (this may only be possible in low-temperature cluster spectroscopy[49,50]).

We show in this work that aniline-d_5 ($C_6D_5NH_2$, abbreviated as An), hydrogen-bonded with two acceptor dimethyl sulfoxide molecules (abbreviated as An···$(DMSO)_2$) with its profound Fermi resonance between N−H stretching fundamental and NH_2 bending first overtone states is an ideal model system to test this hypothesis. We investigate the vibrational energy flow dynamics by use of single- and two-color IR-pump−IR-probe spectroscopy. After introduction of the vibrational level scheme of An and An···$(DMSO)_2$, we present for these two species transient IR spectra of the N−H stretching manifold as well as of the fingerprint region, where the NH_2 bending mode and a ring C═C stretching mode fundamental transition can be found. A combination mode of these two transitions is nearly isoenergetic with the bending overtone and clearly visible in the IR spectra. A comparison will be made for the transient IR response of the NH_2 bending mode under conditions of direct pumping and after pumping the N−H stretching manifold. Ultrafast 2D-IR spectra will be used as support to assess the relative contributions to the pump−probe signals, to indicate connectivities of the different transitions as well as to address the possibility of vibrational excitation transfer within the N−H stretching manifold. Finally, a kinetic fitting procedure of the pump−probe data is used to determine the validity of different IVR scenarios for this hydrogen-bonded system.

EXPERIMENTAL DETAILS

Chemicals. Aniline-d_5 ($C_6D_5NH_2$, 98% atom D), dimethyl sulfoxide (DMSO, purity > 99.8%), and CCl_4 (purity > 99.8%) were obtained from Sigma-Aldrich. DSMO was carefully dried using molecular sieves with pore diameters of 0.3 nm. Solutions were held between CaF_2 windows with Teflon spacers providing path lengths of 20 μm to 10 mm for the FT-IR spectra, of 50−200 μm in the 2D-IR and IR pump−probe measurements, and quartz cells with 10 or 50 mm path length for the overtone spectra. For the time-resolved experiments we have used 0.7 M aniline-d_5 in CCl_4 when probing uncomplexed aniline-d_5, and 0.4 M aniline-d_5 in DMSO, when the double hydrogen-bonded complex was studied.[23]

Steady-State IR Measurements. A Varian 640 FT-IR spectrometer (resolution 1 cm^{-1}) was used to record linear FT-IR spectra in the fundamental N−H stretching and NH_2 bending regions, whereas N−H stretching overtone spectra were measured with a PerkinElmer Lambda 900 spectrometer.

Ultrafast IR Measurements. Femtosecond mid-IR pump−probe and three-pulse 2D-IR photon echo experiments were performed as described previously.[23,24] In short, for the 2D-IR experiments the mid-IR pulses were generated by parametric downconversion of the output of a 1 kHz regeneratively amplified Ti:sapphire laser system providing pulses with a center frequency of 3350 cm^{-1} and 50 fs pulse duration. Two pairs of passively phase-locked pulses with 500 nJ pulse energy each were generated by a diffractive optics setup, and one of those pulses was attenuated by 99% to serve as a local oscillator for spectral interferometric detection of the generated nonlinear

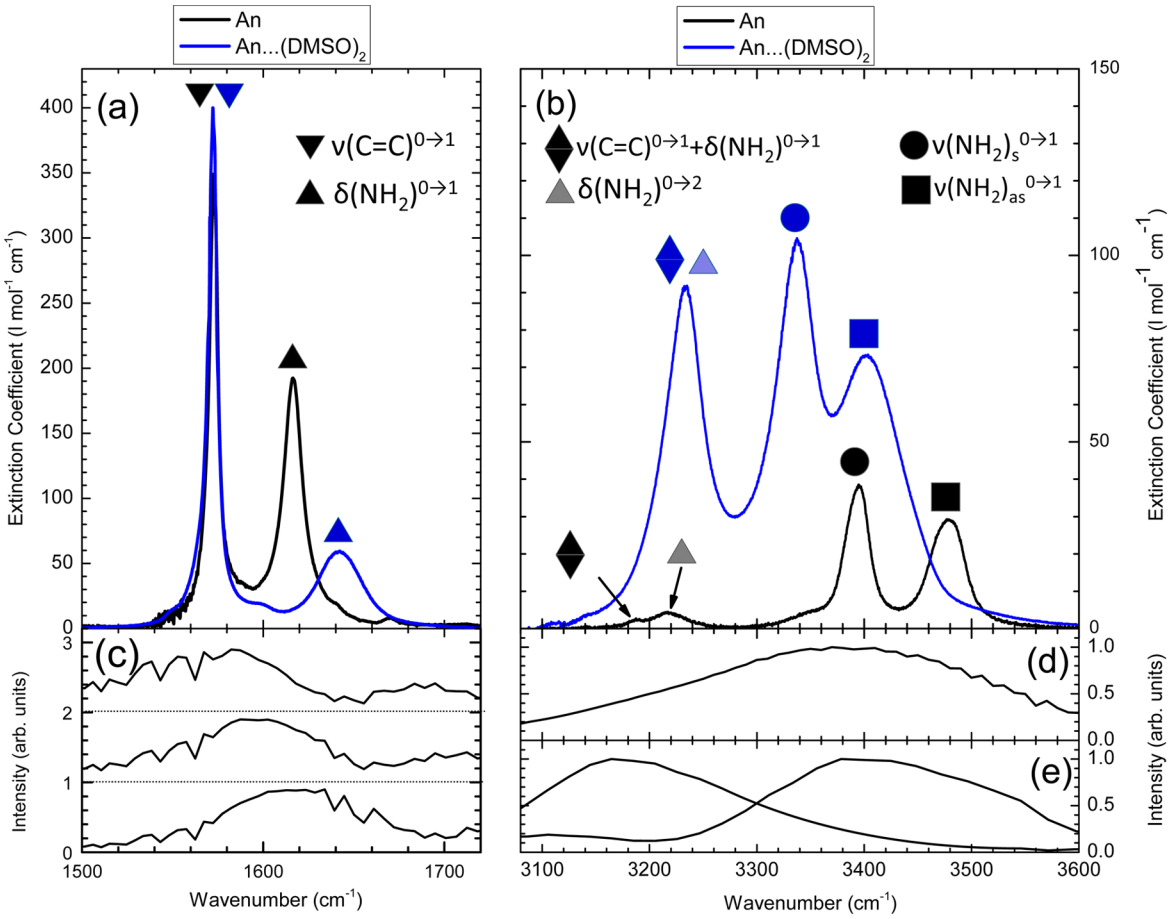

Figure 1. Linear FT-IR spectra of An (black lines) and of An···$(DMSO)_2$ (blue lines) in the fingerprint region (a) and in the N−H stretching region (b). The band assignments are indicated with symbols with the same color coding for the two molecular species. IR laser spectra in the two-color pump−probe (c, e) or single-color pump−probe (d) experiments are shown underneath the FT-IR spectra.

signal. The 2D-IR spectra have a resolution of 4 cm^{-1} along the excitation frequency ν_1 and 9 cm^{-1} along the detection frequency ν_3.

The same setup was used for one-color pump−probe experiments with two of the four pulses blocked while the attenuated probe pulse was detected in a spectrally resolved way to monitor pump-induced absorbance changes in the sample. In contrast, two-color transient absorption measurements were performed with an amplified 1 kHz Ti:sapphire laser system seeding two parametric frequency converters that deliver independently tunable pump and probe pulses with pulse energies of typically 2 μJ and pulse durations of about 100 fs.[24]

INVESTIGATED VIBRATIONAL DEGREES OF FREEDOM OF THE ANILINE-D_5 MODEL SYSTEM

Figure 1 shows the linear FT-IR spectra of An and An···$(DMSO)_2$. The relatively sparse spectra enable a dedicated investigation of the vibrational population dynamics of particular vibrational levels in both the fingerprint and hydrogen stretching regions. To identify which fingerprint vibrations play a dominant role in the Fermi enhancement of the band at 3233 cm^{-1} and estimate the underlying coupling strengths, it turns out that two fingerprint modes have to be regarded: the C═C ring stretching mode ν(C═C) and the NH_2 bending mode $\delta(NH_2)$. A close inspection of linear FT-IR spectra strongly suggests that An (aniline-d_5; $C_6D_5NH_2$) is a better model system than nondeuterated aniline ($C_6H_5NH_2$), due to significantly less mixing of the ν(C═C) ring stretching and the $\delta(NH_2)$ NH_2 bending modes in An (see also Supporting Information). In our previous study of the fundamental and first overtone N−H stretching manifolds,[23] we performed a quantitative analysis of the Fermi enhancement effect of hydrogen bonding on the NH_2 bending overtone for An, An···DMSO, and An···$(DMSO)_2$. The best agreement was obtained with a coupling J between the local N−H stretching modes of −51 cm^{-1} and a coupling V between local N−H stretching modes and the bending overtone of −37 cm^{-1}. The combination tone of the C═C ring stretching mode ν(C═C) and the NH_2 bending mode $\delta(NH_2)$ was disregarded in that analysis. Allowing also for coupling between this combination tone and the N−H stretching modes, the observed oscillator strengths in the N−H stretching region are best reproduced with only minor changes to the coupling parameters J and V (now −52.5 cm^{-1} and −38 cm^{-1}, respectively) and indicates that the coupling between the local N−H stretching mode and the combination tone is about −14 cm^{-1}. Even though the Fermi resonance of the N−H stretching modes with the combination tone is weaker than with the NH_2 bending overtone, this result shows that the transient response of both fingerprint modes should be measured in one- and two-color pump−probe measurements, as both Fermi modes are potentially involved as primary accepting modes in the IVR mechanism of N−H stretching excitation of An.

dx.doi.org/10.1021/jp509977r | J. Phys. Chem. B 2015, 119, 2711−2725

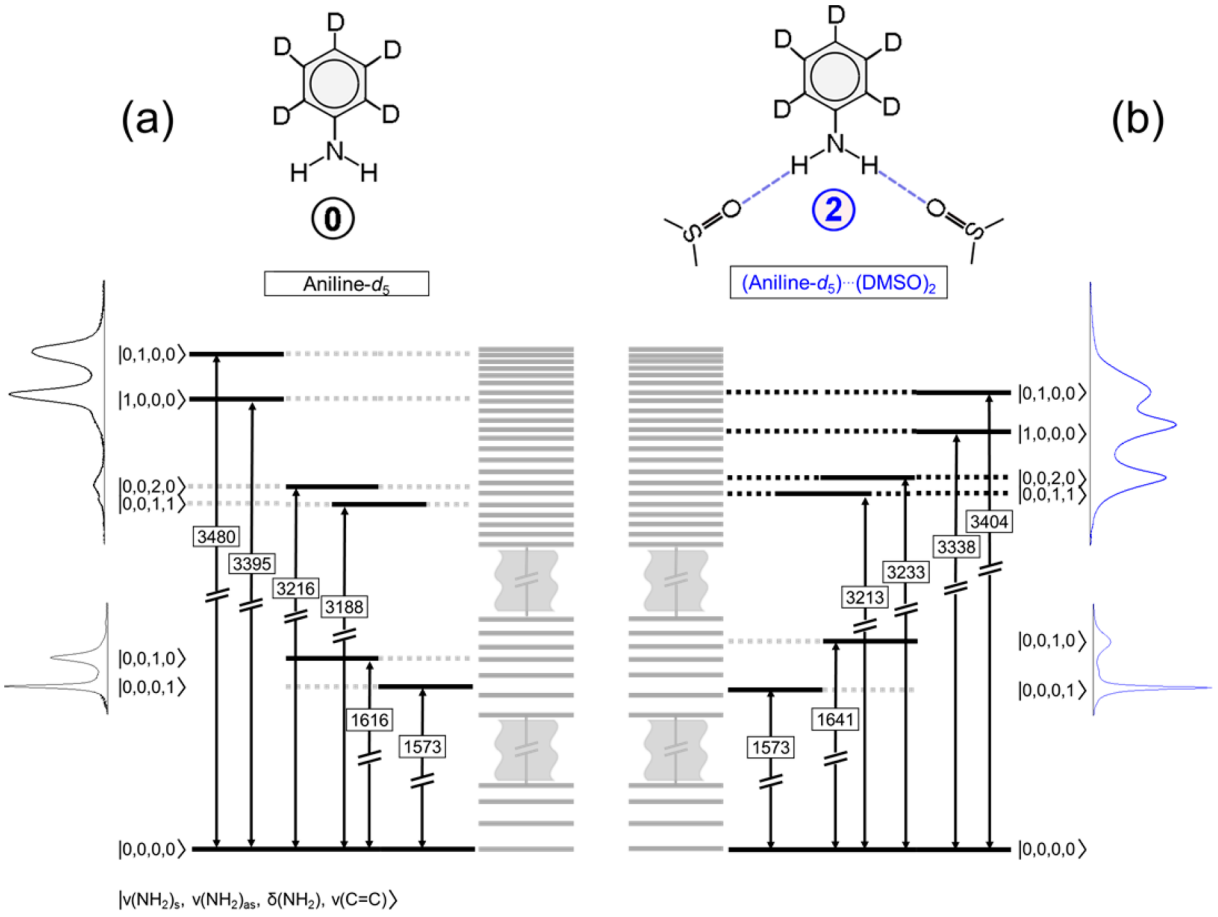

Figure 2. Level schemes of An (a) and of An···$(DMSO)_2$ (b) with associated transition frequencies, together with the molecular structures of An monomer and of the double-hydrogen-bonded complex An···$(DMSO)_2$. The quantum number notation order is for the $|\nu(NH_2)_s, \nu(NH_2)_{as}, \delta(NH_2), \nu(C{=}C)\rangle$ wave function.

Figure 2 thus shows the chemical structures of An and An···$(DMSO)_2$, together with the vibrational level schemes relevant to the ultrafast IR-pump−IR-probe spectroscopic experiments presented here. We consider two fingerprint modes, the C=C ring stretching mode $\nu(C{=}C)$ and the NH_2 bending mode $\delta(NH_2)$, and two N−H stretching modes, that are best described in the normal mode picture, i.e., $\nu(NH_2)_s$ and $\nu(NH_2)_{as}$.[23] Taking into account the Fermi resonances of the N−H stretching modes with the bending overtone, as well as a combination tone of the C=C ring stretching mode $\nu(C{=}C)$ and the NH_2 bending mode $\delta(NH_2)$, we can, with femtosecond IR-pump−IR-probe and 2D-IR photon echo spectroscopy, ideally investigate the vibrational dynamics of a total of six vibrational states (namely, $\{|\nu(NH_2)_{as}{}^1\rangle$, $|\nu(NH_2)_s{}^1\rangle$, $|\delta(NH_2)^2\rangle$, $|\nu(C{=}C)^1\rangle|\delta(NH_2)^1\rangle$, $|\delta(NH_2)^1\rangle$, $|\nu(C{=}C)^1\rangle\}$). With two-color IR-pump−IR-probe spectroscopy we have performed the following three experiments: case I, pump and probe C=C stretching and NH_2 bending mode fundamental transitions in the fingerprint region; case II, pump and probe transitions in the fundamental N−H stretching manifold; case III, pump the fundamental N−H stretching manifold and probe the C=C stretching and NH_2 bending modes in the fingerprint region. Considering the spectral width of the applied IR-pump and IR-probe pulses, the following can be noted. In case I both the C=C stretching $\nu(C{=}C)^{0\rightarrow1}$ and NH_2 bending $\delta(NH_2)^{0\rightarrow1}$ fundamental transitions will simultaneously be excited and probed. For case II, due to the larger bandwidth of the IR pules used, it is to a large extent not possible to preferentially excite either the $\nu(NH_2)_s{}^{0\rightarrow1}$ and $\nu(NH_2)_{as}{}^{0\rightarrow1}$ N−H stretching transitions or the $\delta(NH_2)^{0\rightarrow2}$ NH_2 bending overtone transition, from which individual population lifetimes may be extracted. For case III it is possible to follow the response of the C=C stretching and NH_2 bending modes upon either excitation of the $\nu(NH_2)_s{}^{0\rightarrow1}$ and $\nu(NH_2)_{as}{}^{0\rightarrow1}$ transitions or of the $\delta(NH_2)^{0\rightarrow2}$ overtone transition. With these three cases it is possible to obtain an in-depth picture of the vibrational energy flow in the hydrogen-bonded An···$(DMSO)_2$ complex upon excitation in the N−H stretching manifold.

CASE I: ONE- AND TWO-COLOR PUMP−PROBE EXPERIMENTS ON THE C=C RING STRETCHING MODE $\nu(C{=}C)$ AND THE NH_2 BENDING MODE $\delta(NH_2)$

Parts a and b of Figure 3 show the transient IR pump−probe spectra of An and of An···$(DMSO)_2$, respectively, in the 1540−1700 cm^{-1} frequency range upon excitation of the fingerprint modes. The absorbance change $\Delta A = -\log(T/T_0)$ is plotted as a function of the probe frequency for different pump−probe delays between 0.3 and 9.8 ps (colored lines, T and T_0, sample transmission with and without excitation). The spectra were measured with parallel polarizations of pump and probe. In these measurements bleach signals appear upon excitation at frequency positions of the fundamental transitions of the C=C ring stretching mode $\nu(C{=}C)$ and of the NH_2 bending mode

dx.doi.org/10.1021/jp509977r | J. Phys. Chem. B 2015, 119, 2711−2725

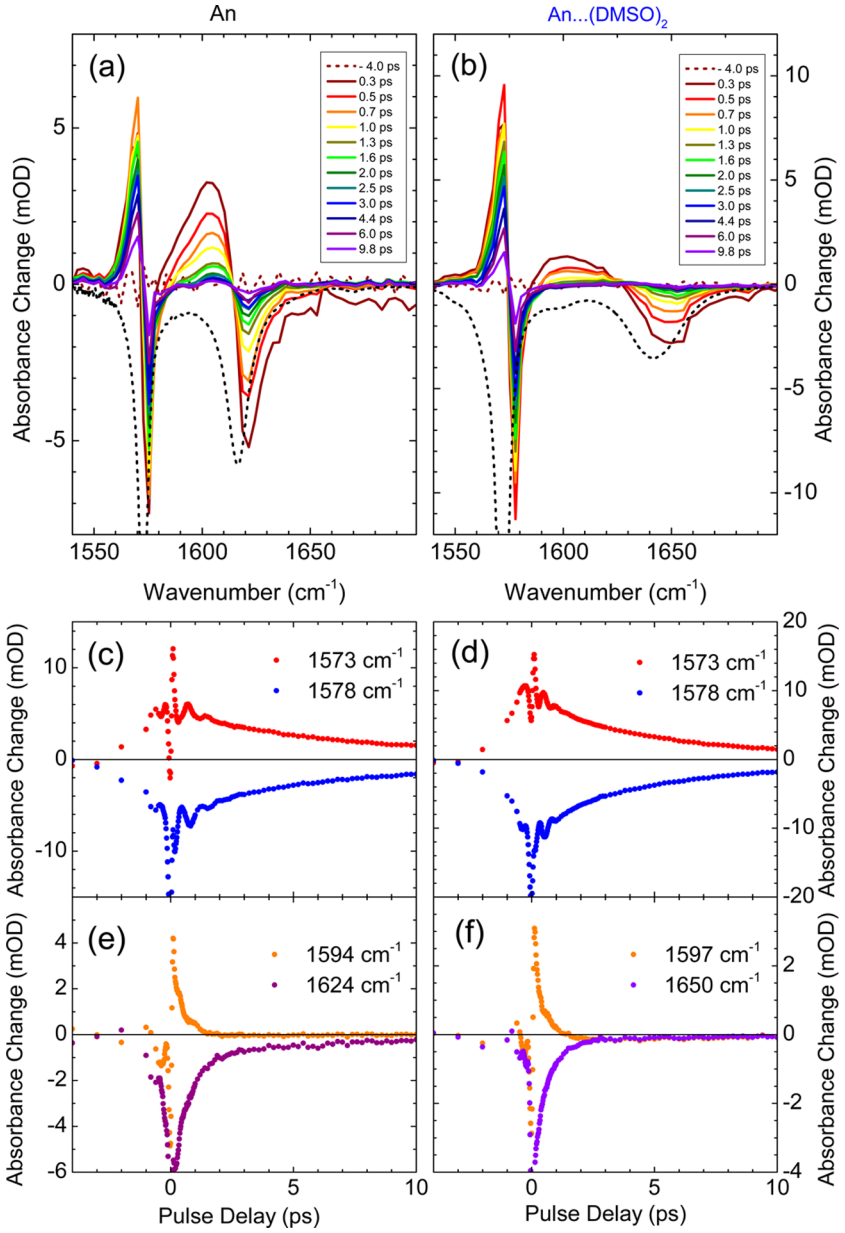

Figure 3. Transient IR pump−probe spectra of the fingerprint modes of An (a) and of An···$(DMSO)_2$ (b) after excitation of the $|\delta(NH_2)^1\rangle$ and $|\nu(CC)^1\rangle$ levels. The steady-state FT-IR spectra are shown on an inverted scale as short dashed lines. The temporal response of the C═C stretching ν(C═C) (c, d) and of the NH_2 bending fundamental (e, f) are shown underneath.

$\delta(NH_2)$, both for An and of An···$(DMSO)_2$. Transient red-shifted absorption is observed for both modes, albeit with different frequency shifts: for the ν(C═C) mode the shift amounts to about 2−3 cm^{-1} for both An and of An···$(DMSO)_2$, and of similar magnitude as the spectral resolution, whereas the frequency shift of transient red-shifted absorption of the $\delta(NH_2)$ mode is 10−15 cm^{-1} for An and 20−30 cm^{-1} for An···$(DMSO)_2$, close to the values of the line width (full width at half-maximum (fwhm)) of the fundamental transitions.

The measured absorbance changes as a function of pulse delay clearly show for both the ground-state bleach recovery and the decay of the red-shifted transient absorption the difference in time scales for the ν(C═C) mode and the $\delta(NH_2)$ mode, both for An (Figure 3c,e) and for An···$(DMSO)_2$ (Figure 3d,f). Whereas for An the ν(C═C) mode bleach and transient red-shifted absorption both decay with an 8.5 ± 0.6 ps time constant, for the $\delta(NH_2)$ mode this time constant is much shorter (0.60 ± 0.05 ps), with an additional second component only for the bleach recovery with a clearly longer 6.8 ± 0.5 ps time constant. An oscillatory component with a period of 43 ± 1 cm^{-1} present on all transient signals of the ν(C═C) mode of An matches the frequency difference between the two fingerprint modes. It has a decay time constant similar to the decay constant of the transient red-shifted absorption of the $\delta(NH_2)$ mode, which has the same oscillatory component as well, albeit with a much smaller relative amplitude. Similar observations can be made for the transient response of these fingerprint modes in An···$(DMSO)_2$. The transient absorption and bleach signals of the ν(C═C) mode decay with a 6.5 ± 0.3 ps time constant. The oscillatory component has a higher frequency of 72 ± 1 cm^{-1}, again determined by the frequency difference of the two

dx.doi.org/10.1021/jp509977r | J. Phys. Chem. B 2015, 119, 2711−2725

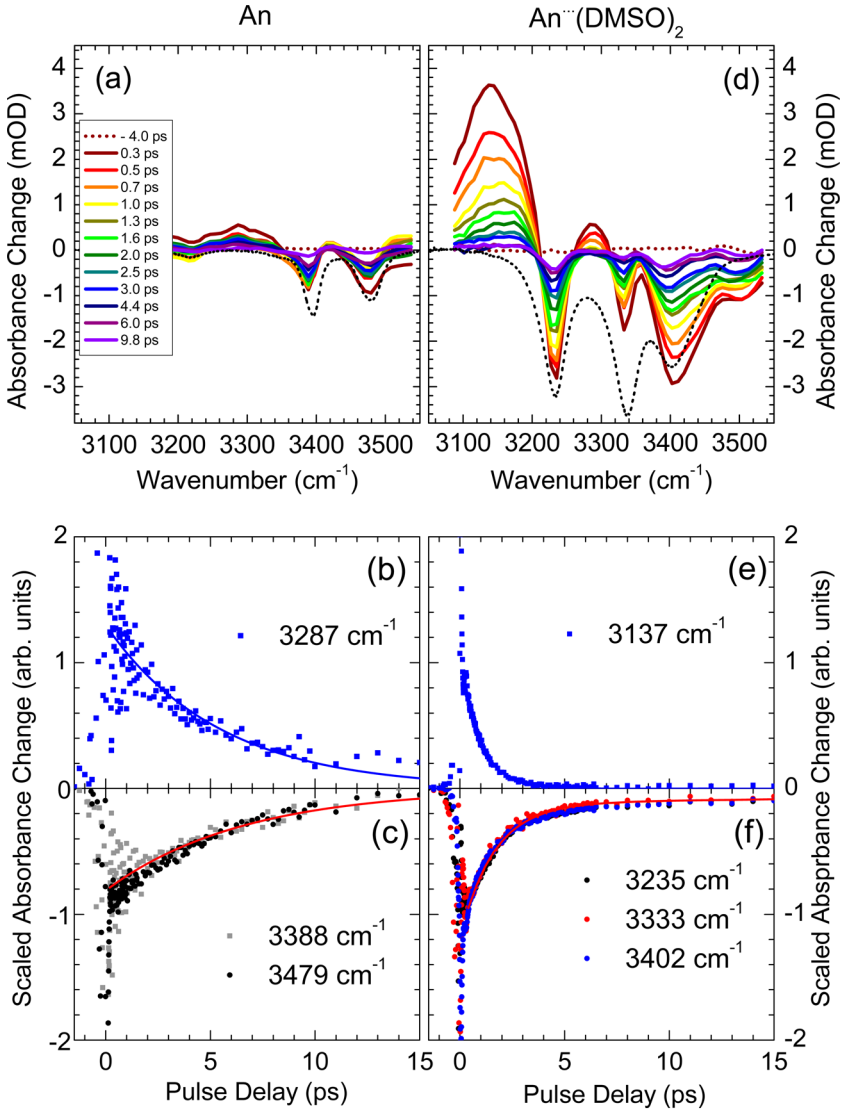

Figure 4. Transient IR pump−probe spectra of the hydrogen stretching manifold of An (a) and of An···$(DMSO)_2$ (d). The steady-state FT-IR spectra are shown on an inverted scale as short dashed lines. The temporal response of excited-state absorption decay (b, e) and of ground-state bleach recovery (c, f) are shown underneath.

fundamental transitions, and shows a slightly shorter decay constant of 0.4 ± 0.1 ps. The decay time constant of the transient absorption of the $\delta(NH_2)$ mode for the hydrogen-bonded complex is 0.44 ± 0.05 ps, and for bleach signals a fast component of 0.50 ± 0.05 ps is found together with an additional slower component of much smaller magnitude with a 6.0 ± 0.5 ps time constant.

The results presented in Figure 3 have been obtained by tuning the excitation pump pulse to halfway in the C═C stretching $\nu(C{=}C)^{0\rightarrow1}$ and NH_2 bending $\delta(NH_2)^{0\rightarrow1}$ fundamental transition frequencies, making the excitation probability of the modes on the same order of magnitude. From these transient IR pump−probe spectra the following can be concluded. For both the $\nu(C{=}C)$ stretching and the $\delta(NH_2)$ bending modes, a bleach (decreased absorbance) at the steady-state C═C stretching $\nu(C{=}C)^{0\rightarrow1}$ and NH_2 bending $\delta(NH_2)^{0\rightarrow1}$ transition frequencies appears within time resolution (which are shown as dashed lines, drawn from inverted FT-IR spectra). Transient red-shifted absorption is also observed within time resolution. Transient red-shifted absorption of a particular vibrational mode in the fingerprint region may have its origin in three different mechanisms:[51,52] (i) red-shifted absorption of the $\nu = 1 \rightarrow \nu = 2$ excited-state absorption of this mode due to diagonal anharmonicity; (ii) instantaneous red-shifted frequency of the unexcited mode, due to off-diagonal anharmonic coupling to another vibrationally excited high-frequency mode; (iii) red-shifted absorption due to the cumulative effect of off-diagonal anharmonic couplings to a multitude of low-frequency modes that are substantially vibrationally excited, in line with a Boltzmann distribution for the molecular system at elevated temperatures.

Option I occurs when pumping directly the C═C stretching $\nu(C{=}C)^{0\rightarrow1}$ or the NH_2 bending $\delta(NH_2)^{0\rightarrow1}$ fundamental transitions in the fingerprint region. Option ii typically applies directly after excitation of a different mode (e.g., the $\nu(NH_2)_s^{0\rightarrow1}$ and $\nu(NH_2)_{as}^{0\rightarrow1}$ transitions or of the $\delta(NH_2)^{0\rightarrow2}$ overtone transition) and causes a mutual red shift of the $\nu(C{=}C)$ and the $\delta(NH_2)$ fingerprint modes with spectrally broad pulses. These features appear directly upon pumping a particular vibrational mode. Subsequent intramolecular vibra-

dx.doi.org/10.1021/jp509977r | J. Phys. Chem. B 2015, 119, 2711−2725

tional energy re-distribution may convert these on a (sub)-picosecond time scale into situation iii where the excess vibrational energy is distributed among many vibrational degrees of freedom of the molecular system. Such a vibrational energy re-distribution results in a Boltzmann distribution for the molecular system at an elevated temperature. Energy dissipation to the solvent, typically slower than the intramolecular vibrational energy re-distribution, leads to vibrational cooling, and the original state of global thermal equilibrium is restored, which for organic solvents such as CCl_4 occurs on a time scale of tens of picoseconds.[32]

The fast component of the transients of the $\delta(NH_2)$ bending mode (0.60 ps in An; 0.44 ps in An···$(DMSO)_2$) can be associated with $\delta(NH_2)$ T_1 population decay of the $|\delta(NH_2)^1\rangle$ state. This short vibrational lifetime is in marked contrast to the population lifetime that can be derived for the $|\nu(C{=}C)^1\rangle$ state: 8.5 ps in An; 6.0 ps in An···$(DMSO)_2$. Note that both the $|\delta(NH_2)^1\rangle$ and $|\nu(C{=}C)^1\rangle$ lifetimes are shortened by about 25% upon the addition of two hydrogen bonds to DMSO molecules. We tentatively ascribe the short $\delta(NH_2)$ bending lifetime to the combined effects of a broader line shape (suggesting more impact of solvent fluctuations) and better frequency matching with combination states of $\beta(NH_2)$ rocking and $\gamma(NH_2)$ wagging modes.[53−56] The fact that the $\delta(NH_2)$ bending mode has a short lifetime both in An and in An···$(DMSO)_2$ excludes a resonance energy transfer mechanism from the bending fundamental state to the S=O stretch/CSC stretch combination state of DMSO. Another consequence of the difference in magnitude of T_1 values for the $\nu(C{=}C)$ stretching and $\delta(NH_2)$ bending modes is that the polarization quantum beat, its frequency equal to the frequency spacing between the two fundamental transitions, can only be observed on the $\nu(C{=}C)$ stretching and $\delta(NH_2)$ bending transient signals for the duration of the $|\delta(NH_2)^1\rangle$ state. The fact that this quantum beat is more pronounced in the $\nu(C{=}C)$ stretching transient signals than in those of the $\delta(NH_2)$ bending mode is due to the latter mode having a broader line shape, whereas small frequency modulations can be more easily observed in the spectrally narrower $\nu(C{=}C)$ stretching signals. For the fraction of molecules where the $\delta(NH_2)^{0\rightarrow1}$ transition occurs, the $\delta(NH_2)$ bending decay dynamics is reflected in the minor frequency upshift of ∼2.5 cm^{-1} of the $\nu(C{=}C)$ stretching mode on the same time scale. From this we can conclude that the effects of red-shifted absorption of the $\nu(C{=}C)$ stretching mode due to reaching a hot ground state after $\delta(NH_2)$ bending decay is even smaller than the spectral resolution of 2.5 cm^{-1}. For the fraction of molecules where the $\nu(C{=}C)^{0\rightarrow1}$ transition occurs, the anharmonic coupling to the $\delta(NH_2)$ bending mode is reflected in the long time component of the bleach signal.

The clear difference of an order of magnitude in the decay time of the C=C stretching and NH_2 bending modes allows for a profound insight into the magnitude of diagonal and off-diagonal anharmonicities of these fingerprint modes. In the results obtained from An monomer, we derive a diagonal anharmonicity as defined as $\Delta_{21} = \nu^{1\rightarrow2} - \nu^{0\rightarrow1}$, for the $\nu(C{=}C)$ stretching mode of Δ_{21} = 3.5 ± 1.0 cm^{-1} (for both An and An···$(DMSO)_2$) and for the $\delta(NH_2)$ bending mode to be Δ_{21} = 12 ± 3 cm^{-1} (An) and Δ_{21} = 25 ± 5 cm^{-1} (An···$(DMSO)_2$). These values can be compared with the magnitude of the anharmonic coupling between the C=C stretching and NH_2 bending modes of about 2.5 cm^{-1}, and the effects of frequency red-shifting of "hot" ground states that are <2.5 cm^{-1}. The relevance of these findings for case I will become clear when we present and discuss the results of case III. Before doing that, we have to determine the vibrational population kinetics of the N−H stretching manifold, i.e., case II, that will be discussed in the next section.

CASE II: ONE-COLOR PUMP−PROBE AND 2D-IR EXPERIMENTS ON THE N−H STRETCHING MODES $\nu(NH_2)_S$ AND $\nu(NH_2)_{AS}$ AND THE NH_2 BENDING RELATED COMBINATION/OVERTONE MODES

Parts a and b of Figure 4 show the transient IR spectra of An and of An···$(DMSO)_2$ after excitation in the N−H stretching manifold. The bandwidth of the IR pump and probe pulses was large, resulting in the simultaneous excitation and probing of all transitions within the Fermi combination/overtone/N−H stretching manifold. These pump−probe signals have been recorded for perpendicular pump and probe pulse polarization condition, but no significant differences were observed for pump−probe measurement results with parallel polarization condition. Bleach signals can be observed at the fundamental $\nu(NH_2)_s^{0\rightarrow1}$ and $\nu(NH_2)_{as}^{0\rightarrow1}$ transition frequencies for both uncomplexed An and hydrogen-bonded An···$(DMSO)_2$, as well as for the Fermi resonance enhanced band that can be associated with the $\delta(NH_2)^{0\rightarrow2}$ NH_2 bending overtone and the $\nu(C{=}C)^{0\rightarrow1}\delta(NH_2)^{0\rightarrow1}$ combination tone. The smaller signals for uncomplexed An compared to those for hydrogen-bonded An···$(DMSO)_2$ are a consequence of the smaller transition dipole moments for the $\nu(NH_2)_s^{0\rightarrow1}$ and $\nu(NH_2)_{as}^{0\rightarrow1}$ transitions in free An. Red-shifted transient absorption is observed as well. Referring to our previously published 2D-IR spectra,[23] these transient absorbance signals can be assigned either to excited-state absorption ($\nu(NH_2)_s^{1\rightarrow2}$ and $\nu(NH_2)_{as}^{1\rightarrow2}$ transitions) or to red-shifted absorption from excited N−H stretching v = 1 states to combination states within the first stretching overtone manifold by anharmonically coupled N−H stretching vibrations or to transitions where the NH_2 bending $|\delta(NH_2)^2\rangle$ overtone state and/or $|\nu(C{=}C)^1\rangle|\delta(NH_2)^1\rangle$ combination state is involved.

Taking into account the limited signal-to-noise ratio of the transient signals for An monomer, a T_1 population decay time constant of 5 ± 1 ps results from fitting the excited-state absorption signal at 3287 cm^{-1} (signal dominated by contributions from the $\nu(NH_2)_s^{1\rightarrow2}$ transition). Knowing that the vibrational cooling rates in molecules dissolved in CCl_4 are on the order of tens of picoseconds, the longer values for the time constants of bleach recovery of 6.7 ± 0.5 ps (3388 cm^{-1}; $\nu(NH_2)_s^{0\rightarrow1}$ transition) and 6.4 ± 0.5 ps (3479 cm^{-1}; $\nu(NH_2)_{as}^{0\rightarrow1}$ transition) may hint at the occurrence of a "hot" ground state reached after population relaxation of the v = 1 N−H stretching states. Whereas the excited-state decay and bleach recovery of the N−H stretching transitions clearly lie in the picosecond range for uncomplexed An, the increase of vibrational relaxation rates of the N−H stretching v = 1 states in hydrogen-bonded complexes An···$(DMSO)_2$ is in line with previously published literature on vibrational relaxation of hydrogen stretching modes in hydrogen-bonded molecular systems.[57] As such it is of no surprise to deduce a significantly shorter excited-state absorption time constant of 0.9 ± 0.3 ps at 3137 cm^{-1} (signal dominated by contributions from the $|\nu(NH_2)_{as}^1\rangle$ to the $|\nu(NH_2)_{as}^1\rangle|\delta(NH_2)^2\rangle$ combination state), or an even shorter excited-state absorption time constant of 0.5 ± 0.3 ps at 3300 cm^{-1} (signal dominated by contributions from

dx.doi.org/10.1021/jp509977r | J. Phys. Chem. B 2015, 119, 2711−2725

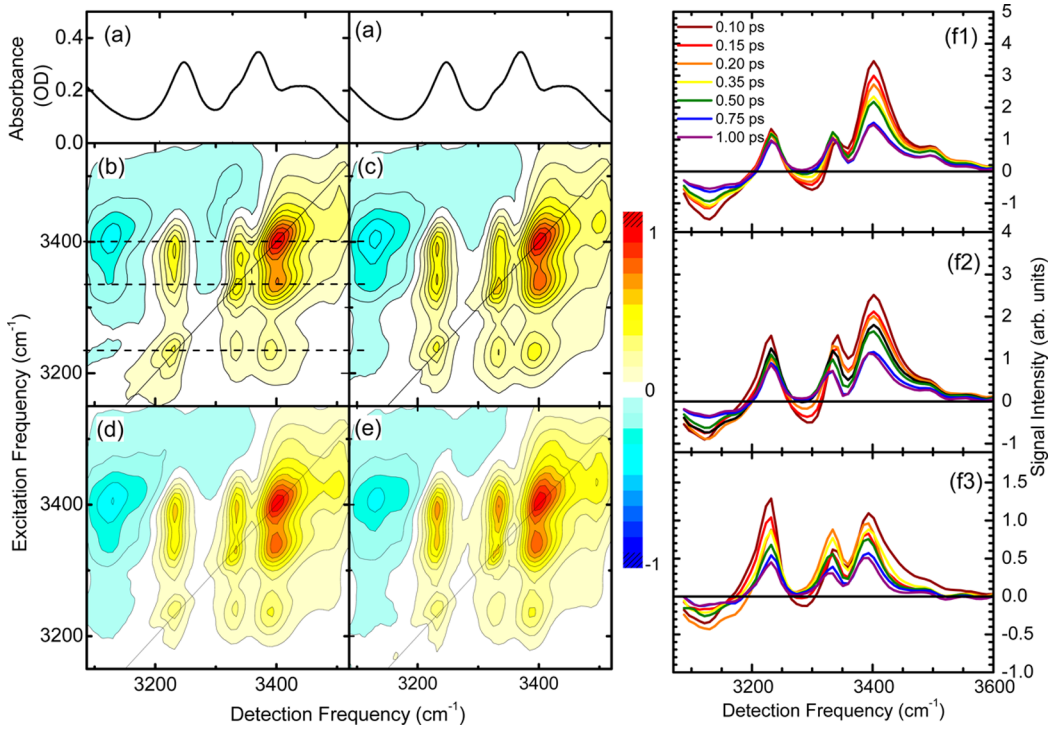

Figure 5. Absorptive 2D-IR spectra of An···$(DMSO)_2$ showing the overall decay dynamics out of the N−H stretching manifold for population (waiting) time T = (b) 150, (c) 350, (d) 500, and (e) 1000 fs. Panel a shows the linear FT-IR spectrum of An···$(DMSO)_2$. Panels f1−f3 show the temporal behavior of the nonlinear signals along the detection frequency axis for specific excitation frequencies of (f1) 3400, (f2) 3348, and (f3) 3237 cm^{-1} as a function of the population waiting time T.

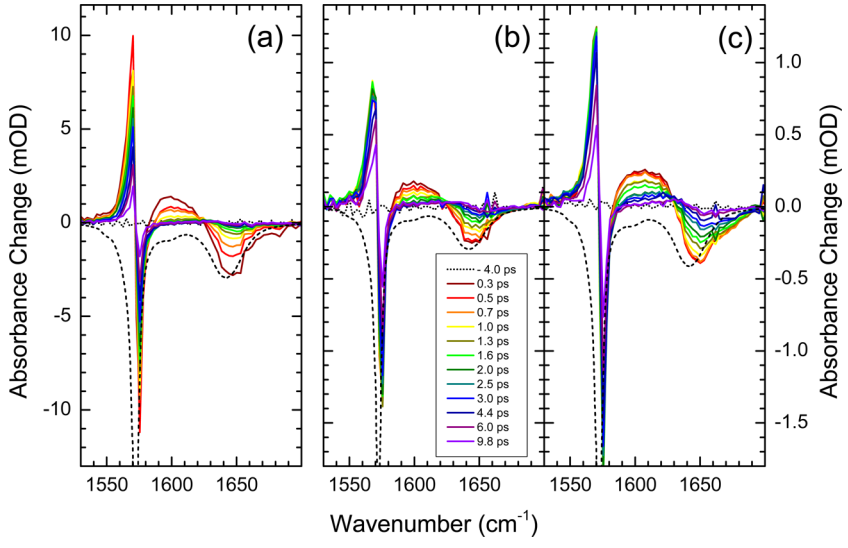

Figure 6. Transient IR pump−probe spectra of An···$(DMSO)_2$, for different IR pump tuning: (a) pump tuned at fundamental transitions of the fingerprint modes (1597 cm^{-1}); (b) pump tuned at NH_2 bending combination/overtone transition (3170 cm^{-1}); (c) pump centered at the N−H stretching transitions (3401 cm^{-1}). For pulse pump spectra see Figure 1c,e.

the transition of the $|\delta(NH_2)^2\rangle$ bending overtone state to the $|\nu(NH_2)_s^1\rangle|\delta(NH_2)^2\rangle$ combination state and from the transition of the $|\nu(NH_2)_s^1\rangle$ fundamental state to the $|\nu(NH_2)_s^1\rangle|\nu(NH_2)_{as}^1\rangle$ combination state, with a smaller role for the transition from $|\nu(NH_2)_{as}^1\rangle$ to the $|\nu(NH_2)_{as}^2\rangle$ overtone state). From these observations we deduce vibrational lifetimes of the different states within the N−H stretching manifold to lie in the 0.5−0.9 ps range. Ground-state recovery is better reproduced with biexponential fitting, resulting in time constants of 1.1 ± 0.3 ps with a longer 7.8 ± 0.5 ps component (3235 cm^{-1}; NH_2 bending $\delta(NH_2)^{0\to2}$ overtone and/or $\nu(C{=}C)^{0\to1}\delta(NH_2)^{0\to1}$ combination tone transition), 1.6 ± 0.3 ps (3333 cm^{-1}; $\nu(NH_2)_s^{0\to1}$ transition), and 1.2 ± 0.3 ps with a longer 6.5 ± 0.5 ps component (3402 cm^{-1}; $\nu(NH_2)_{as}^{0\to1}$ transition). In particular, the longer 6−8 ps time component may—again—hint at the role of frequency-shifted hot ground-state absorption after population relaxation of the N−H stretching manifold states to lower frequency modes in the fingerprint region and beyond.

dx.doi.org/10.1021/jp509977r | J. Phys. Chem. B 2015, 119, 2711−2725

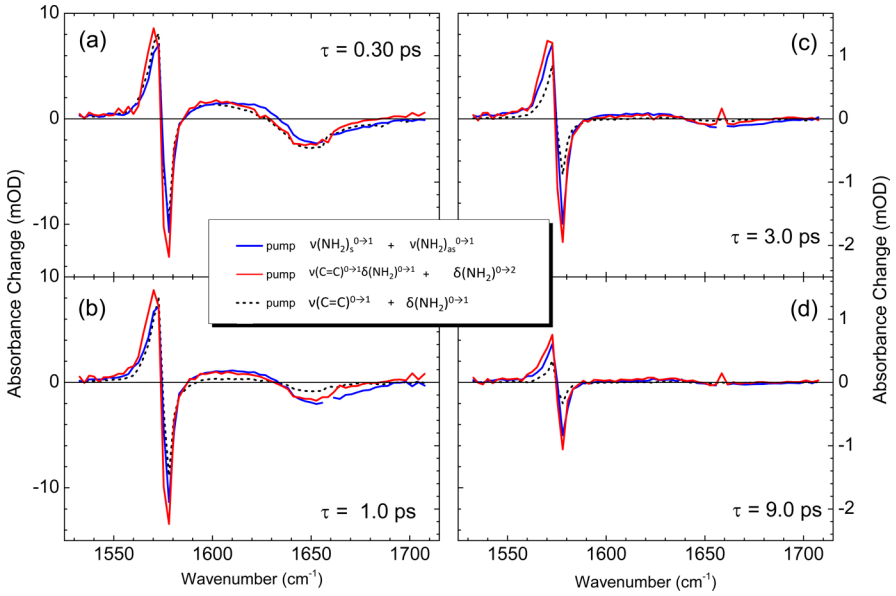

Figure 7. Comparison of the IR pump−probe spectra for different excitation conditions, exemplifying the variation in excited-state absorption at early pulse delay, similarities at later times, and differences in the magnitude of the transient population in the ν(C═C) stretching mode at longer picosecond pulse delay. Scaling of the two-color IR pump−probe signals for the two different excitation conditions was achieved by equating the NH_2 bending $\delta(NH_2)^{0\rightarrow1}$ ground-state bleach signal. The left axis denotes the absorbance change upon excitation of the fingerprint modes (black dashed lines). The right axis denotes the absorbance change upon excitation of the Fermi enhanced combination/overtone transitions (red lines; multiplication factor, 1.667) or of the N−H stretching transitions (blue lines).

The measured pump−probe data suggest not an overtly different decay rate for the stretching mode and bending overtone/combination tone excited states $\{|\nu(NH_2)_{as}{}^1\rangle$, $|\nu(NH_2)_s{}^1\rangle$, $|\delta(NH_2)^2\rangle$, $|\nu(C{=}C)^1\rangle|\delta(NH_2)^1\rangle\}$. Figure 5 shows measured 2D-IR spectra for (ZZXX) polarization conditions (i.e., having pulses 1 and 2 with polarization directions orthogonal to those of pulse 3 and the local oscillator) as a function of the population (waiting) time T for An···$(DMSO)_2$. A similar overall decay in magnitude occurs for diagonal and negative off-diagonal peaks, suggesting similar T_1 population decay times. Having similar decay dynamics out of the $\{|\nu(NH_2)_{as}{}^1\rangle$, $|\nu(NH_2)_s{}^1\rangle$, $|\delta(NH_2)^2\rangle$, $|\nu(C{=}C)^1\rangle|\delta(NH_2)^1\rangle\}$ states will prevent an observation of a significant transient population buildup of the Fermi resonance enhanced overtone/combination tone states $\{|\delta(NH_2)^2\rangle$, $|\nu(C{=}C)^1\rangle|\delta(NH_2)^1\rangle\}$ upon feeding from the N−H stretching states $\{|\nu(NH_2)_{as}{}^1\rangle$, $|\nu(NH_2)_s{}^1\rangle\}$, and one cannot distinguish between IVR pathways from the N−H stretching states $\{|\nu(NH_2)_{as}{}^1\rangle$, $|\nu(NH_2)_s{}^1\rangle\}$ directly to the fundamental fingerprint states $\{|\delta(NH_2)^1\rangle$, $|\nu(C{=}C)^1\rangle\}$ or via the fingerprint overtone/combination tone states $\{|\delta(NH_2)^2\rangle$, $|\nu(C{=}C)^1\rangle|\delta(NH_2)^1\rangle\}$.

CASE III: TWO-COLOR PUMP−PROBE EXPERIMENTS SHOWING THE CONNECTIVITIES BETWEEN THE N−H STRETCHING $\nu(NH_2)_S$ AND $\nu(NH_2)_{AS}$ MODES AND THE C═C RING STRETCHING MODE ν(C═C) AND THE NH_2 BENDING MODE $\delta(NH_2)$

We have recorded two-color transient IR spectra, monitoring the response of the fingerprint modes under pump excitation conditions where predominantly either the N−H stretching fundamentals or the Fermi enhanced combination/overtone transitions are initially populated. In Figures 6 and 7 we depict our results for these two different case III two-color pump−probe measurements in direct comparison to the single-color pump−probe measurements of the fingerprint modes of case I, to emphasize the close similarity in the number of spectral components in these transient vibrational responses. Figure 6 shows a comparison of the transient IR spectra of the fingerprint modes of An···$(DMSO)_2$ for the three different excitation conditions: (a) either the $|\nu(C{=}C)^1\rangle$ or the $|\delta(NH_2)^1\rangle$ has been excited (this plot is identical to Figure 3b); (b) either the $|\delta(NH_2)^2\rangle$ overtone or the $|\nu(C{=}C)^1\rangle|\delta(NH_2)^1\rangle$ combination levels have been excited; (c) either the N−H stretching $|\nu(NH_2)_s{}^1\rangle$ or the N−H stretching $|\nu(NH_2)_{as}{}^1\rangle$ has been pumped. Differences in the transient response of the ν(C═C) stretching and $\delta(NH_2)$ bending modes become only apparent when looking closely to the dynamical behavior. Whereas in Figure 6a the transient red-shifted absorption of the fingerprint modes appears within time resolution and decays subsequently with the respective vibrational population lifetimes of the $|\nu(C{=}C)^1\rangle$ and $|\delta(NH_2)^1\rangle$ states, excitation of the Fermi enhanced bending overtone/combination tone or of the N−H stretching modes both indicate a more delayed decaying of these fingerprint modes. This is particularly clear for the ν(C═C) stretching mode (Figure 6b,c), which itself decays slow relative to the feeding time from the stretching manifold decay. To interpret the observed vibrational dynamics, we need to estimate relative contributions to the transient absorbance signals in the case III experiments. To assist in this, we have taken transient IR spectra for the three different excitation conditions (as depicted in Figure 6), all rescaled to the NH_2 bending bleach signal at pulse delay τ = 300 fs, and show the comparative spectral signatures for the ν(C═C) stretching and $\delta(NH_2)$ bending modes for a few chosen pulse delay times in Figure 7.

Upon excitation of the N−H stretching/Fermi bending overtone/combination manifold around 3200−3450 cm^{-1} with the IR pump pulse, transient excited-state absorption to the combinational levels located between 4700 and 5100 cm^{-1} can

dx.doi.org/10.1021/jp509977r | J. Phys. Chem. B 2015, 119, 2711−2725

be expected to occur as long as T_1 population decay has not taken place. To assist in this assessment, we have recorded the IR absorption spectrum in this spectral range (see Supporting Information, Figure S3 and Table S2). The observed combination bands appear to show a pronounced frequency downshift upon hydrogen bonding, indicating the key role of the N−H stretching degrees of freedom in this spectral region. Using this spectral information on the combination bands, one can obtain an estimate where transient excited-state absorption of the IR-probe pulse is expected upon excitation in the N−H stretching manifold. It follows that the anharmonic shift between the NH_2 bending or the ν(C═C) stretching on the one side and the symmetric and asymmetric N−H stretching $\nu(NH_2)_s$ and $\nu(NH_2)_{as}$ on the other side is of minor magnitude for An···$(DMSO)_2$, i.e. ,<10 cm^{-1}. The consequence is that excitation of the $|\nu(NH_2)_s{}^1\rangle$ and the $|\nu(NH_2)_{as}{}^1\rangle$ N−H stretching states results in transient absorption of the fingerprint modes only slightly red-shifted from the ground-state bleach contribution to an extent governed by the instantaneous anharmonic shift (i.e., <10 cm^{-1}). For vibrational modes with transitions with similar or smaller spectral widths, such instantaneous frequency red shifts can be observed with femtosecond pump−probe spectroscopy, whereas for broad transitions (with spectral widths much larger than the anharmonic frequency shifts) the transient absorption and bleach components nearly cancel. As a result, the observed red-shifted transient absorption for the ν(C═C) stretching mode (fwhm = 6 cm^{-1}) may at early times be interpreted as instantaneous anharmonic shifted absorption from the excited modes within the N−H stretching/N−H bending combination/overtone manifold. In contrast, the assignment of combinational levels in the 4760−5100 cm^{-1} range suggests that the observable red-shift of the NH_2 bending mode (fwhm = 33 cm^{-1}) due to N−H stretching excitation is significantly less than the ∼50 cm^{-1} red shift of the $\delta(NH_2)^{1\rightarrow2}$ transition relative to the fundamental $\delta(NH_2)^{0\rightarrow1}$ transition. This is confirmed by the data in Figure 7, which show that after 0.3 ps the cancellation point (excited-state absorption equals ground-state bleach) lies at significantly higher frequency when the N−H the stretching modes are initially excited, compared to initial excitation of the Fermi bands near 3200 cm^{-1} or the bending fundamental, which have cancellation at a similar frequency. After 1 ps both traces after excitation of the N−H stretching modes and after excitation of predominant Fermi modes have the same cancellation frequency, illustrating that the v = 1 levels of the N−H stretching modes are essentially depleted after 1 ps.

For the $|\delta(NH_2)^2\rangle$ overtone state, a $\delta(NH_2)^{0\rightarrow1}$ ground-state bleach contribution at 1641 cm^{-1} will be accompanied by a $\delta(NH_2)^{2\rightarrow1}$ stimulated emission contribution located at 1592 cm^{-1}. For this $\delta(NH_2)^{2\rightarrow1}$ stimulated emission contribution, significant cancellation can be expected by the $\delta(NH_2)^{2\rightarrow3}$ excited-state absorption which should occur at even lower frequencies.

Figures 6 and 7 show that after a picosecond the transient IR spectra appear rather similar, notwithstanding the different excitation conditions. We ascribe this behavior to a buildup of similar relative populations of the $|\nu(C{=}C)^1\rangle$ and $|\delta(NH_2)^1\rangle$ states after excitation of the $|\delta(NH_2)^2\rangle$ overtone and the $|\nu(C{=}C)^1\rangle>|\delta(NH_2)^1\rangle$ combination levels, or of the $|\nu(NH_2)_s{}^1\rangle$ and the $|\nu(NH_2)_{as}{}^1\rangle$ N−H stretching states, however with a delayed rise for these excitation conditions compared to direct excitation in the fingerprint region. This conclusion is further substantiated by the observation that for An···$(DMSO)_2$ decay dynamics of the transient spectra for the ν(C═C) stretching and $\delta(NH_2)$ bending mode region in Figure 6 panels a−c have become very similar after a picosecond. This means a fast population decay of the $|\delta(NH_2)^1\rangle$ state, with almost complete red-shifted absorption decay and bleach recovery. The minor component shown on picosecond times scales reflects the anharmonic shift of the NH_2 bending $\delta(NH_2)$ mode due to the vibrationally excited ν(C═C) stretching mode, in a way similar to that as concluded for case I. The transient red-shifted absorption and associated bleach of the fundamental $\nu(C{=}C)^{0\rightarrow1}$ transition on picosecond time scales indicates the transient population of the $|\nu(C{=}C)^1\rangle$ state (accompanied by vibrational cooling dynamics as exemplified by the small frequency upshifting of the excited-state absorption). Parts b−d of Figure 7 illustrate once more that for both the NH_2 bending and the ν(C═C) stretching mode the transient red-shifted absorption decay and transient bleach recovery is delayed for initial excitations in the NH_2 stretching manifold.

We furthermore observe that the magnitude of the resulting response in the fingerprint modes is similar for excitation in different regions within the N−H stretching manifold. This suggests also that the subsequent IVR follows similar pathways resulting in a similar transient first excited-state population of the ν(C═C) stretching and the $\delta(NH_2)$ bending modes about a picosecond after the primary excitation events. Consequently, it is very likely that the population decay of the excited N−H stretching modes occurs via the bending overtone state $|\delta(NH_2)^2\rangle$ and the combination mode $|\nu(C{=}C)^1\rangle|\delta(NH_2)^1\rangle$. A kinetic analysis of the transient IR absorbance features is needed to illustrate if key insights into the primary vibrational energy flow pathways can be extracted with more certainty.

KINETIC ANALYSIS OF VIBRATIONAL ENERGY FLOW IN AN AND AN···$(DMSO)_2$

We have plotted the time dependence of the signals of the two fingerprint modes in An···$(DMSO)_2$ in Figure 8 for the three excitation conditions also presented in Figure 6. For longer pulse delay times than about 1−2 ps the transient red-shifted absorptions at 1568 and at 1602 cm^{-1} can be interpreted as a direct indicator for the degree of vibrational excitation of the $|\nu(C{=}C)^1\rangle$ and $|\delta(NH_2)^1\rangle$ states, respectively. At earlier times in the two-color pump−probe (case III) experiments, these spectral signatures reflect a complex population dynamics within the higher lying N−H stretching/NH_2 bending combination/overtone manifold, followed by cooling of low-frequency modes within the first excited state of these fingerprint modes. Focusing on the population dynamics after the coherent artifact (pulse delay times, τ > 0.3 ps) we point to the delayed buildup of signal for the ν(C═C) stretching mode upon excitation of the NH_2 bending combination/overtone levels, which becomes even more pronounced if the N−H stretching levels are initially populated. For the $\delta(NH_2)$ bending mode the signal does not increase with pulse delay. However, the decay is significantly slower following excitation of the NH_2 bending combination/overtone levels than after direct excitation of the bending fundamental transition. Upon excitation of the N−H stretching modes the decay is significantly slower during the first picosecond, whereafter it becomes identical to the decay rate following excitation of the Fermi enhanced NH_2 bending combination/overtone modes.

dx.doi.org/10.1021/jp509977r | J. Phys. Chem. B 2015, 119, 2711−2725

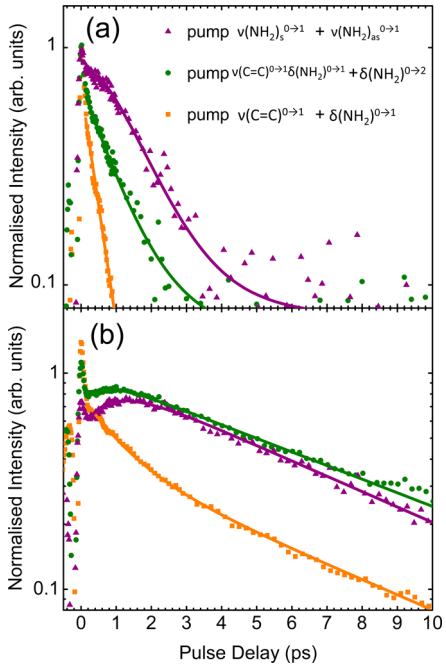

Figure 8. Transient dynamics of red-shifted absorption of the NH_2 bending (a; signal at 1602 cm^{-1}) and of the ν(C═C) stretching (b; signal at 1568 cm^{-1}) modes for different tuning of the IR pump pulses (purple triangles, pump the $\nu(NH_2)_s^{0\to1}$ and $\nu(NH_2)_{as}^{0\to1}$ N−H stretching transitions; olive circles, pump the $\delta(NH_2)^{0\to2}$ NH_2 bending overtone and the $\nu(C{=}C)^{0\to1}\delta(NH_2)^{0\to1}$ combination tone; orange squares, pump the $\nu(C{=}C)^{0\to1}$ and $\delta(NH_2)^{0\to1}$ fundamental fingerprint transitions), shown on a logarithmic scale. Multiexponential fits are shown as solid lines.

Multiexponential fitting enables an insight into the time scales of the IVR process in the An···$(DMSO)_2$ complex (see Figure 8). Population decay of the $|\delta(NH_2)^1\rangle$ state can be fitted with the T_1 population lifetime component value of 0.44 ± 0.05 ps. Note that the kinetic behavior of the $|\delta(NH_2)^1\rangle$ population is more accurately reflected by the excited-state absorption signal than by the ground-state recovery signal. Following excitation in the Fermi enhanced combination/overtone levels the transient absorption signal decay slows to 0.95 ± 0.1 ps. The same 0.95 ps decay time is found after initial excitation of the N−H stretching levels, but in this case an additional rise time component with time constant 0.6 ± 0.2 ps is needed to accurately mimic the slower decay during the first picosecond. These data strongly suggest that the decay of the N−H stretching modes goes via the Fermi enhanced levels.

As already mentioned under case I, the T_1 population lifetime of the $|\delta(NH_2)^1\rangle$ state for the An monomer in CCl_4 is 0.60 ± 0.05 ps, about a third longer than in An···$(DMSO)_2$. For the An monomer the time-resolved experiment with only excitation in the Fermi enhanced combination/overtone levels cannot be performed, due to the much weaker absorption of the Fermi bands the signal would still be dominated by the stretching mode response. Following direct excitation of the $|\nu(NH_2)_{as}^1\rangle$ and $|\nu(NH_2)_s^1\rangle$ N−H stretching states the transient population of the $|\delta(NH_2)^1\rangle$ state of An monomer shows a signal decaying with a single time constant of 6 ± 1 ps, which roughly matches the 5 ± 1 ps T_1 lifetime mentioned in case II for a signal dominated by the $|\nu(NH_2)_s^1\rangle$ state (Figure 9). As the lifetime of the $|\delta(NH_2)^1\rangle$ state is only 0.6 ps, the response of the $|\delta(NH_2)^1\rangle$ state following excitation of the N−H stretching states is clearly governed by the much slower feeding rate provided by the excited-state decay of states $|\nu(NH_2)_{as}^1\rangle$ and $|\nu(NH_2)_s^1\rangle$.

Population decay following direct excitation of the $|\nu(C{=}C)^1\rangle$ state in An···$(DMSO)_2$ can be fitted with the T_1 population lifetime component 6.5 ± 0.3 ps, with an additional faster 1.0 ± 0.2 ps component related to the contribution of the

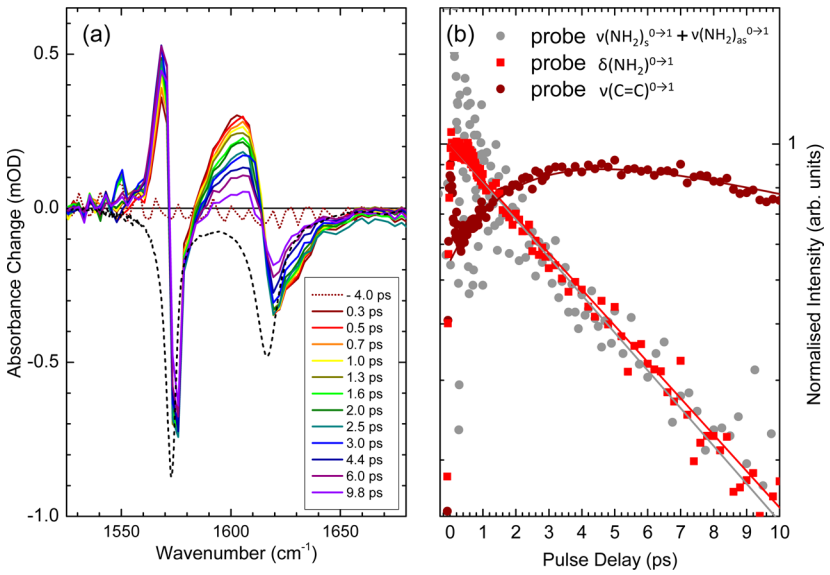

Figure 9. (a) Transient IR pump−probe spectra of the fingerprint modes of An after excitation of the $|\nu(NH_2)_s^1\rangle$ and $|\nu(NH_2)_{as}^1\rangle$ levels. The steady-state FT-IR spectra are shown on an inverted scale as short dashed lines. (b) Transient dynamics of red-shifted absorption, shown on a logarithmic scale, of the NH_2 bending (red squares; signal at 1605 cm^{-1}) coincides with the transient population kinetics measured in the N−H stretching manifold (gray dots; measured at 3287 cm^{-1}). The kinetics of the NH_2 bending mode follows an exponential decay behavior with a 6 ± 1 ps time constant, close to the 5 ± 1 ps excited-state decay of the N−H stretching mode. The red-shifted absorption of the ν(C═C) stretching mode (brown dots; signal at 1571 cm^{-1}) on the other hand shows an increase with a 5.7 ps time constant, followed by a slower decay with a 13 ± 1 ps constant governed by the ν(C═C) stretching exicted-state population decay.

dx.doi.org/10.1021/jp509977r | J. Phys. Chem. B 2015, 119, 2711−2725

quantum beat with the $|\delta(NH_2)^1\rangle$ state (~2 T_1). Following excitation of the Fermi enhanced combination/overtone levels a rise component with a time constant of 0.6 ± 0.1 ps is followed by a decay with 7 ± 1 ps. Upon excitation of the N−H stretching levels the rise component is clearly more pronounced with a slightly longer time constant of 0.8 ± 0.1 ps, and followed by a similar 7 ± 1 ps decay, suggesting only a marginal difference in arrival time in the $|\nu(C{=}C)^1\rangle$ state between initial excitation of the N−H stretching or the NH_2 bending related combination/overtone levels.

As mentioned under case I, for the An monomer in CCl_4 the T_1 population lifetime of the $|\nu(C{=}C)^1\rangle$ state is 8.5 ± 0.5 ps. Following direct excitation of the $|\nu(NH_2)_{as}^1\rangle$ and $|\nu(NH_2)_s^1\rangle$ N−H stretching states the excited-state absorption from the $|\nu(C{=}C)^1\rangle$ state shows a strongly frequency-dependent rise with a time constant of 2.2 ps at 1566 cm^{-1} and gradually increasing to 5.7 ps at 1573 cm^{-1}, in each case followed by an exponential decay with a time constant of 13 ± 1 ps at all detection frequencies (see Figure 9). The frequency-dependent rise is likely related to cooling of low-frequency modes that are simultaneously populated with the $|\nu(C{=}C)^1\rangle$ state by the decay from the N−H stretching levels and lead to a larger red shift of the $|\nu(C{=}C)^1\rangle$ state by their coupling to this mode. Both the slowest 5.7 ps rise time and the increase of the slow component from 8.5 ps for direct excitation of the $|\nu(C{=}C)^1\rangle$ state to 13 ps are in line with a feeding rate dominated by the 5 ± 1 ps lifetime of the N−H stretching modes, that also explained the 6 ± 1 ps component in the decay of the $|\delta(NH_2)^1\rangle$ state after excitation of these modes.

The obtained results provide convincing evidence for an IVR pathway scheme in the An···$(DMSO)_2$ complex, based on routing of vibrational excitations within the N−H stretching/NH_2 bending combination/overtone manifold toward the $|\nu(C{=}C)^1\rangle$ and $|\delta(NH_2)^1\rangle$ states. The results for the An···$(DMSO)_2$ complex show that the feeding of the $|\nu(C{=}C)^1\rangle$> and $|\delta(NH_2)^1\rangle$ states is (somewhat) slower upon excitation of the $|\nu(NH_2)_{as}^1\rangle$ and $|\nu(NH_2)_s^1\rangle$ N−H stretching states than upon excitation of the $|\delta(NH_2)^2\rangle$ and $|\nu(C{=}C)^1{>}|\delta(NH_2)^1\rangle$ combination/overtone states, which strongly suggests that the decay of the N−H stretching states occurs via these combination/overtone states. However, it is not possible to determine with certainty whether the higher lying N−H stretching level excitations directly feed the NH_2 bending combination/overtone levels, and these subsequently decay into the first excited states of the fingerprint modes, or whether the N−H stretching excitations directly feed the $|\nu(C{=}C)^1\rangle$ and $|\delta(NH_2)^1\rangle$ states. This is a consequence of the similar decay rates of these different levels within the N−H stretching/NH_2 bending combination/overtone manifold, which prevents a significant transient population build-up in the NH_2 bending combination/overtone levels. For the An monomer selective excitation of these combination/overtone levels was not possible, and data with excitation of the $\nu(NH_2)_{as}^1\rangle$ and $|\nu(NH_2)_s^1\rangle$ states demonstrate that the transient population dynamics of both the $|\nu(C{=}C)^1\rangle$ and $|\delta(NH_2)^1\rangle$ states is governed by the N−H stretching population lifetime, which are about an order of magnitude longer in An monomer than in the double-hydrogen-bonded An···$(DMSO)_2$ complex. The fact that in the An···$(DMSO)_2$ complex IVR from the N−H stretching levels results in significant population of both the $|\nu(C{=}C)^1\rangle$ and $|\delta(NH_2)^1\rangle$ states, with a similar relative population ratio, suggests that in both cases routing occurs via the $|\delta(NH_2)^2\rangle$ overtone and $|\nu(C{=}C)^1\rangle|\delta(NH_2)^1\rangle$ combination tone states toward the $|\nu(C{=}C)^1\rangle$ and $|\delta(NH_2)^1\rangle$ states. Hydrogen bonding thus appears to enhance the rates of already existing IVR pathways.

Further analysis of the IVR dynamics for the An···$(DMSO)_2$ complex using appropriate modeling of the transient population kinetics within the N−H stretching manifold and the two fingerprint fundamental levels suggests the following. Direct excitation of the Fermi enhanced $|\delta(NH_2)^2\rangle$ overtone and $|\nu(C{=}C)^1\rangle|\delta(NH_2)^1\rangle$ combination tone states would prepare the molecular system with a population distribution, in accordance with the excitation efficiency as dictated by the respective IR cross-sections and the pump pulse spectrum. Regardless of the actual prepared state, the first step in vibrational re-distribution will be the conversion of one quantum of NH_2 bending into other low-frequency vibrational excitations. The argument behind this is that the decay rate of the Fermi enhanced combination/overtone states is similar to or faster than the 0.44 ps (An···$(DMSO)_2$) or 0.60 ps (An) decay rate of the $|\delta(NH_2)^1\rangle$ state. In contrast, the much slower decay of the $\nu(C{=}C)$ stretching mode indicates a smaller involvement in the initial step of IVR from the combination state. Thus, the decay rate out of the overtone and combination tone states is similar, and decay of the $|\nu(C{=}C)^1\rangle|\delta(NH_2)^1\rangle$ state is expected to predominantly feed the $|\nu(C{=}C)^1\rangle$ level, whereas decay of the $|\delta(NH_2)^2\rangle$ overtone level will mostly be reflected in the $|\delta(NH_2)^1\rangle$ population kinetics. Based on this the relative magnitude of spectral changes of the $\nu(C{=}C)$ stretching and $\delta(NH_2)$ bending modes in the fingerprint region are a direct reflection of the initially prepared population in the Fermi enhanced overtone/combination tone states, provided no ultrafast population exchange between the Fermi enhanced overtone/combination tone states occurs within the population lifetime.

A surprising result is that the transient responses of the $\nu(C{=}C)$ stretching and $\delta(NH_2)$ bending modes in the fingerprint region are also similar when excitation of the N−H stretching modes is induced by the IR pump pulse. One cannot a priori exclude that the $|\nu(NH_2)_s^1\rangle$ and $|\nu(NH_2)_{as}^1\rangle$ states of the N−H stretching modes directly relax to the $|\nu(C{=}C)^1\rangle$ or $|\delta(NH_2)^1\rangle$ states, because the appearance in these fundamental states of the fingerprint modes is delayed compared to the case when the Fermi enhanced combination/overtone states are excited. However, given the similarities in relative yield in the transient population of the $|\nu(C{=}C)^1\rangle$ and $|\delta(NH_2)^1\rangle$ states and similarities in absolute signal strength between initial excitation of the N−H stretching modes versus the combination/overtone states, it seems highly unlikely that decay from the $|\nu(NH_2)_s^1\rangle$ and $|\nu(NH_2)_{as}^1\rangle$ states occurs with equal opportunity to all combination/overtone states in the vibrational manifold roughly matching the energy of the N−H stretching modes. Note also that the Fermi enhancement upon hydrogen bonding implies that mixing occurs between the $|\nu(NH_2)_s^1\rangle$ and $|\nu(NH_2)_{as}^1\rangle$ states and the states $|\delta(NH_2)^2\rangle$ and $|\nu(C{=}C)^1{>}|\delta(NH_2)^1\rangle$, for which we determined coupling constants of −37 and −14 cm^{-1}, respectively. On the basis of this inherent mixing, we argue that a routing from the N−H stretching states to these Fermi enhanced combination/overtone states, rather than an indiscriminate ejection into the vibrational manifold, is the more likely IVR pathway following excitation of the N−H stretching states $|\nu(NH_2)_s^1\rangle$ and $|\nu(NH_2)_{as}^1\rangle$.

dx.doi.org/10.1021/jp509977r | J. Phys. Chem. B 2015, 119, 2711−2725

CONCLUSION

We have presented an ultrafast IR pump−probe and 2D-IR photon echo study of intramolecular vibrational energy flow in a model system for the Fermi resonance between N−H stretching modes and modes involving the NH_2 bending, in which hydrogen bonding strongly enhances the impact of this type of vibrational coupling on IR cross-sections and IVR pathways and associated dynamics. Building on our previously reported linear and nonlinear IR study on aniline-d_5 (An) hydrogen-bonded to dimethyl sulfoxide (DMSO), we are able to identify the primary IVR channels for excitation of the N−H stretching/NH_2 bending combination/overtone manifold of the An···$(DMSO)_2$ complex in CCl_4. An interesting feature is that hydrogen bonding of aniline-d_5 results in marked changes in frequency positions and in IR cross-sections within the N−H stretching manifold, accompanied by drastic changes in N−H stretching vibrational lifetimes from ∼5 to ∼1 ps. Instead the changes upon hydrogen bonding in the $\delta(NH_2)$ bending mode position and lifetimes (from 0.60 to 0.44 ps) are somewhat smaller, whereby it should be noticed that its lifetime is already very short for the An monomer. For the ν(C═C) stretching mode the position change is negligible, and a small reduction in lifetime from 8.5 to 6.5 ps is found.. The primary event of vibrational energy flow from the N−H stretching/NH_2 bending combination/overtone manifold occurs into two fingerprint modes, namely, the ν(C═C) stretching mode and the $\delta(NH_2)$ bending mode, that play a key role in the Fermi resonances with the N−H stretching modes. From this it immediately follows that the primary events in IVR after excitation of the N−H stretching manifold leads to molecular states that are far from a situation where the internal molecular vibration excitation can be described using a Boltzmann distribution consistent with an elevated temperature. This is further corroborated by the fact that the$|\nu(C{=}C)^1\rangle$ lifetime is an order of magnitude longer than the $|\delta(NH_2)^1\rangle$ lifetime. This finding is fully consistent with results from other ultrafast vibrational spectroscopic studies of hydrogen-bonded systems.[36−38,43] For An the obtained data sets suggest that the same IVR pathways exist as in the double-hydrogen-bonded An···$(DMSO)_2$ complex. From this we learn that hydrogen bonding enhances vibrational decay rates for N−H stretching excitations in already existing IVR pathways.

Comparison of the time scales for the delayed appearance of population in the v = 1 states of the ν(C═C) stretching and $\delta(NH_2)$ bending modes upon excitation of the N−H stretching states or upon excitation of the Fermi enhanced combination/overtone states is consistent with a vibrational relaxation mechanism where the N−H stretching excitation follows an IVR pathway via the Fermi resonance enhanced combination/overtone states. Despite this strong indication, it is not possible to unequivocally identify the relaxation route for N−H stretching excitations as exclusively going via the Fermi enhanced combination/overtone states. Here we are hampered by the fact that population relaxation rates out of the $|\nu(NH_2)_{as}^1\rangle$> and $|\nu(NH_2)_s^1\rangle$ N−H stretching states are similar to or slower than those out of the $|\delta(NH_2)^2\rangle$ and $|\nu(C{=}C)^1\rangle|\delta(NH_2)^1\rangle$ combination/overtone states, preventing a significant transient population build-up in the combination/overtone states, when pumping the N−H stretching states. However, the surprising outcome of this study is that the transient population of the $|\nu(C{=}C)^1\rangle$ and $|\delta(NH_2)^1\rangle$ states is of similar magnitude, regardless of the excitation conditions within the N−H stretching manifold. This strongly suggests that for reaching the fundamentally excited ν(C═C) stretching and $\delta(NH_2)$ bending states, IVR pathways from the $|\nu(NH_2)_{as}^1\rangle$ and $|\nu(NH_2)_s^1\rangle$ N−H stretching states or from the $|\delta(NH_2)^2\rangle$ and $|\nu(C{=}C)^1\rangle|\delta(NH_2)^1\rangle$ combination/overtone states have a common underlying mechanism. Our obtained results on the ultrafast IVR dynamics in this model system for hydrogen bonding enhancement of Fermi resonances will have general relevance for other hydrogen-bonded molecular systems, including DNA bases.

ASSOCIATED CONTENT

Supporting Information

Text describing comparison between vibrational modes in aniline-h_7 and in aniline-d_5, combination tone spectroscopy of aniline-d_5, and accompanying references, figures showing linear IR spectra, and tables listing vibration band positions and assignments. This material is available free of charge via the Internet at http://pubs.acs.org.

AUTHOR INFORMATION

Corresponding Author

*Email: nibberin@mbi-berlin.de.

Notes

The authors declare no competing financial interest.

ACKNOWLEDGMENTS

This research has received funding from the European Research Council under the European Union's Seventh Framework Programme (FP7/2007-2013)/ERC Grant Agreement No. 247051.

REFERENCES

(1) Fermi, E. Über den Ramaneffekt des Kohlendioxyds. *Z. Phys.* **1931**, *71*, 250−259.

(2) Sheppard, N. Infrared Spectroscopy and Hydrogen Bonding—Band-Widths and Frequency Shifts. In *Hydrogen Bonding*; Hadži, D., Thompson, H. W., Eds.; Pergamon Press: New York, 1959; pp 85−105.

(3) Hadži, D.; Bratos, S. Vibrational Spectroscopy of the Hydrogen Bond. In *The Hydrogen Bond: Recent Developments in Theory and Experiments*; Schuster, P., Zundel, G., Sandorfy, C., Eds.; North Holland: Amsterdam, The Netherlands, 1976; Vol. *II*, Structure and Spectroscopy, pp 565−611.

(4) Henri-Rousseau, O.; Blaise, P. The Infrared Spectral Density of Weak Hydrogen Bonds within the Linear Response Theory. *Adv. Chem. Phys.* **1998**, *103*, 1−186.

(5) Henri-Rousseau, O.; Blaise, P.; Chamma, D. Infrared Lineshapes of Weak Hydrogen Bonds: Recent Quantum Developments. *Adv. Chem. Phys.* **2002**, *121*, 241−309.

(6) Halonen, L. Local Mode Vibrations in Polyatomic Molecules. *Adv. Chem. Phys.* **1998**, *104*, 41−179.

(7) Marechal, Y.; Witkowski, A. Infrared Spectra of H-Bonded Systems. *J. Chem. Phys.* **1968**, *48*, 3697−3705.

(8) Maréchal, Y. IR Spectra of Carboxylic Acids in the Gas Phase: A Quantitative Reinvestigation. *J. Chem. Phys.* **1987**, *87*, 6344−6353.

(9) Häber, T.; Schmitt, U.; Emmeluth, C.; Suhm, M. A. Ragout-Jet FTIR Spectroscopy of Cluster Isomerism and Cluster Dynamics: From Carboxylic Acid Dimers to N_2O Nanoparticles. *Faraday Discuss.* **2001**, *118*, 331−359.

(10) Emmeluth, C.; Suhm, M. A. A Chemical Approach Towards the Spectroscopy of Carboxylic Acid Dimer Isomerism. *Phys. Chem. Chem. Phys.* **2003**, *5*, 3094−3099.

(11) Emmeluth, C.; Suhm, M. A.; Luckhaus, D. A Monomers-in-Dimers Model for Carboxylic Acid Dimers. *J. Chem. Phys.* **2003**, *118*, 2242−2255.
(12) Huse, N.; Heyne, K.; Dreyer, J.; Nibbering, E. T. J.; Elsaesser, T. Vibrational Multi-Level Quantum Beats Due to Anharmonic Couplings in Intermolecular Hydrogen Bonds. *Phys. Rev. Lett.* **2003**, *91*, No. 197401.
(13) Heyne, K.; Huse, N.; Dreyer, J.; Nibbering, E. T. J.; Elsaesser, T.; Mukamel, S. Coherent Low-Frequency Motions of Hydrogen Bonded Acetic Acid Dimers in the Liquid Phase. *J. Chem. Phys.* **2004**, *121*, 902−913.
(14) Huse, N.; Bruner, B. D.; Cowan, M. L.; Dreyer, J.; Nibbering, E. T. J.; Miller, R. J. D.; Elsaesser, T. Anharmonic Couplings Underlying Ultrafast Vibrational Dynamics of Hydrogen Bonds in Liquids. *Phys. Rev. Lett.* **2005**, *95*, No. 147402.
(15) Dreyer, J. Hydrogen-Bonded Acetic Acid Dimers: Anharmonic Coupling and Linear Infrared Spectra Studied with Density-Functional Theory. *J. Chem. Phys.* **2005**, *122*, No. 184306.
(16) Dreyer, J. Density Functional Theory Simulations of Two-Dimensional Infrared Spectra for Hydrogen-Bonded Acetic Acid Dimers. *Int. J. Quantum Chem.* **2005**, *104*, 782−793.
(17) Dwyer, J. R.; Dreyer, J.; Nibbering, E. T. J.; Elsaesser, T. Ultrafast Dynamics of Vibrational N-H Stretching Excitations in the 7-Azaindole Dimer. *Chem. Phys. Lett.* **2006**, *432*, 146−151.
(18) Dreyer, J. Unraveling the Structure of Hydrogen Bond Stretching Mode Infrared Absorption Bands: An Anharmonic Density Functional Theory Study on 7-Azaindole Dimers. *J. Chem. Phys.* **2007**, *127*, No. 054309.
(19) Wassermann, T. N.; Rice, C. A.; Suhm, M. A.; Luckhaus, D. Hydrogen Bonding Lights up Overtones in Pyrazoles. *J. Chem. Phys.* **2007**, 127.
(20) Szyc, Ł.; Guo, J.; Yang, M.; Dreyer, J.; Tolstoy, P. M.; Nibbering, E. T. J.; Czarnik-Matusewicz, B.; Elsaesser, T.; Limbach, H.-H. The Hydrogen-Bonded 2-Pyridone Dimer Model System. 1. Combined NMR and FT-IR Study. *J. Phys. Chem. A* **2010**, *114*, 7749−7760.
(21) Yang, M.; Szyc, Ł.; Dreyer, J.; Nibbering, E. T. J.; Elsaesser, T. The Hydrogen-Bonded 2-Pyridone Dimer Model System. 2. Femtosecond Mid-Infrared Pump-Probe Study. *J. Phys. Chem. A* **2010**, *114*, 12195−12201.
(22) Kiefer, P. M.; Hynes, J. T. Theoretical Aspects of Tunneling Proton Transfer Reactions in a Polar Environment. *J. Phys. Org. Chem.* **2010**, *23*, 632−646.
(23) Greve, C.; Nibbering, E. T. J.; Fidder, H. Hydrogen-Bonding-Induced Enhancement of Fermi Resonances: A Linear IR and Nonlinear 2D-IR Study of Aniline-d_5. *J. Phys. Chem. B* **2013**, *117*, 15843−15855.
(24) Greve, C.; Preketes, N. K.; Fidder, H.; Costard, R.; Koeppe, B.; Heisler, I. A.; Mukamel, S.; Temps, F.; Nibbering, E. T. J.; Elsaesser, T. N-H Stretching Excitations in Adenosine-Thymidine Base Pairs in Solution: Pair Geometries, Infrared Line Shapes, and Ultrafast Vibrational Dynamics. *J. Phys. Chem. A* **2013**, *117*, 594−606.
(25) Oxtoby, D. W. Vibrational Population Relaxation in Liquids. *Adv. Chem. Phys.* **1981**, *47*, 487−519.
(26) Oxtoby, D. W. Vibrational Relaxation in Liquids. *Annu. Rev. Phys. Chem.* **1981**, *32*, 77−101.
(27) Nesbitt, D. J.; Field, R. W. Vibrational Energy Flow in Highly Excited Molecules: Role of Intramolecular Vibrational Redistribution. *J. Phys. Chem.* **1996**, *100*, 12735−12756.
(28) Gruebele, M. Vibrational Energy Flow: A State Space Approach. *Adv. Chem. Phys.* **2000**, *114*, 193−261.
(29) Leitner, D. M. Heat Transport in Molecules and Reaction Kinetics: The Role of Quantum Energy Flow and Localization. In *Advances in Chemical Physics, Geometric Structures of Phase Space in Multidimensional Chaos: Applications to Chemical Reaction Dynamics in Complex Systems, Part B*; Toda, M., Komatsuzaki, T., Konishi, T., Rice, S. A., Eds.; Wiley: Hoboken, NJ, USA, 2005; Vol. *130*, pp 205−256.
(30) Leitner, D. M.; Matsunaga, Y.; Li, C.-B.; Komatsuzaki, T.; Shojiguchi, A.; Toda, M.Non-Brownian Phase Space Dynamics of Molecules, the Nature of Their Vibrational States, and Non-RRKM Kinetics. *Advances in Chemical Physics, Advancing Theory for Kinetics and Dynamics of Complex, Many-Dimensional Systems: Clusters and Proteins*; Wiley: Hoboken, NJ, USA, 2011; Vol. *145*, pp 83−122.
(31) Elsaesser, T.; Kaiser, W. Vibrational and Vibronic Relaxation of Large Polyatomic Molecules in Liquids. *Annu. Rev. Phys. Chem.* **1991**, *42*, 83−107.
(32) Owrutsky, J. C.; Raftery, D.; Hochstrasser, R. M. Vibrational Relaxation Dynamics in Solutions. *Annu. Rev. Phys. Chem.* **1994**, *45*, 519−555.
(33) Laubereau, A.; Fischer, S. F.; Spanner, K.; Kaiser, W. Vibrational Population Lifetimes of Polyatomic Molecules in Liquids. *Chem. Phys.* **1978**, *31*, 335−344.
(34) Fendt, A.; Fischer, S. F.; Kaiser, W. Vibrational Lifetime and Fermi Resonance in Polyatomic-Molecules. *Chem. Phys.* **1981**, *57*, 55−64.
(35) Dlott, D. D. Vibrational Energy Redistribution in Polyatomic Liquids: 3D Infrared-Raman Spectroscopy. *Chem. Phys.* **2001**, *266*, 149−166.
(36) Kozich, V.; Dreyer, J.; Ashihara, S.; Werncke, W.; Elsaesser, T.; Mode-Selective, O.-H. Mode-Selective O−H Stretching Relaxation in a Hydrogen Bond Studied by Ultrafast Vibrational Spectroscopy. *J. Chem. Phys.* **2006**, *125*, No. 074504.
(37) Kozich, V.; Dreyer, J.; Werncke, W. Mode-Selective Vibrational Redistribution after Spectrally Selective N-H Stretching Mode Excitation in Intermolecular Hydrogen Bonds. *J. Chem. Phys.* **2009**, *130*, No. 034505.
(38) Kozich, V.; Szyc, Ł.; Nibbering, E. T. J.; Werncke, W.; Elsaesser, T. Ultrafast Redistribution of Vibrational Energy after Excitation of NH Stretching Modes in DNA Oligomers. *Chem. Phys. Lett.* **2009**, *473*, 171−175.
(39) Salmi, T.; Haenninen, V.; Garden, A. L.; Kjaergaard, H. G.; Tennyson, J.; Halonen, L. Calculation of the O−H Stretching Vibrational Overtone Spectrum of the Water Dimer. *J. Phys. Chem. A* **2008**, *112*, 6305−6312.
(40) Salmi, T.; Kjaergaard, H. G.; Halonen, L. Calculation of Overtone O−H Stretching Bands and Intensities of the Water Trimer. *J. Phys. Chem. A* **2009**, *113*, 9124−9132.
(41) Sälli, E.; Salmi, T.; Halonen, L. Computational High-Frequency Overtone Spectra of the Water−Ammonia Complex. *J. Phys. Chem. A* **2011**, *115*, 11594−11605.
(42) Cringus, D.; Lindner, J.; Milder, M. T. W.; Pshenichnikov, M. S.; Vöhringer, P.; Wiersma, D. A. Femtosecond Water Dynamics in Reverse-Micellar Nanodroplets. *Chem. Phys. Lett.* **2005**, *408*, 162−168.
(43) Ashihara, S.; Huse, N.; Espagne, A.; Nibbering, E. T. J.; Elsaesser, T. Ultrafast Structural Dynamics of Water Induced by Dissipation of Vibrational Energy. *J. Phys. Chem. A* **2007**, *111*, 743−746.
(44) Costard, R.; Elsaesser, T. Femtosecond OH Bending Dynamics of Water Nanopools Confined in Reverse Micelles. *J. Phys. Chem. B* **2013**, *117*, 15338−15345.
(45) Rey, R.; Møller, K. B.; Hynes, J. T. Ultrafast Vibrational Population Dynamics of Water and Related Systems: A Theoretical Perspective. *Chem. Rev.* **2004**, *104*, 1915−1928.
(46) Schäfer, T.; Lindner, J.; Vöhringer, P.; Schwarzer, D. OD Stretch Vibrational Relaxation of HOD in Liquid to Supercritical H_2O. *J. Chem. Phys.* **2009**, *130*, No. 224502.
(47) Deàk, J. C.; Iwaki, L. K.; Dlott, D. D. Vibrational Energy Redistribution in Polyatomic Liquids: Ultrafast IR-Raman Spectroscopy of Acetonitrile. *J. Phys. Chem. A* **1998**, *102*, 8193−8201.
(48) Deàk, J. C.; Iwaki, L. K.; Dlott, D. D. Vibrational Energy Redistribution in Polyatomic Liquids: Ultrafast IR-Raman Spectroscopy of Nitromethane. *J. Phys. Chem. A* **1999**, *103*, 971−979.
(49) Robertson, W. H.; Johnson, M. A. Molecular Aspects of Halide Ion Hydration: The Cluster Approach. *Annu. Rev. Phys. Chem.* **2003**, *54*, 173−213.
(50) Robertson, W. H.; Price, E. A.; Weber, J. M.; Shin, J. W.; Weddle, G. H.; Johnson, M. A. Infrared Signatures of a Water Molecule Attached to Triatomic Domains of Molecular Anions:

Evolution of the H-Bonding Configuration with Domain Length. *J. Phys. Chem. A* **2003**, *107*, 6527−6532.
(51) Hamm, P.; Ohline, S. M.; Zinth, W. Vibrational Cooling after Ultrafast Photoisomerization of Azobenzene Measured by Femtosecond Infrared Spectroscopy. *J. Chem. Phys.* **1997**, *106*, 519−529.
(52) Nibbering, E. T. J.; Fidder, H.; Pines, E. Ultrafast Chemistry: Using Time-Resolved Vibrational Spectroscopy for Interrogation of Structural Dynamics. *Annu. Rev. Phys. Chem.* **2005**, *56*, 337−367.
(53) Tzeng, W. B.; Narayanan, K.; Shieh, K. C.; Tung, C. C. A Study of the Structures and Vibrations of $C_6H_5NH_2$, C_6H_5NHD, $C_6H_5ND_2$, $C_6D_5NH_2$, C_6D_5NHD, and $C_6D_5ND_2$ in the S_1 State by Ab Initio Calculations. *J. Mol. Struct. (THEOCHEM)* **1998**, *428*, 231−240.
(54) Piest, H.; von Helden, G.; Meijer, G. Infrared Spectroscopy of Jet-Cooled Neutral and Ionized Aniline-Ar. *J. Chem. Phys.* **1999**, *110*, 2010−2015.
(55) Gée, C.; Douin, S.; Crépin, C.; Bréchignac, P. Infrared Spectroscopy of Aniline ($C_6H_5NH_2$) and Its Cation in a Cryogenic Argon Matrix. *Chem. Phys. Lett.* **2001**, *338*, 130−136.
(56) Wojciechowski, P. M.; Zierkiewicz, W.; Michalska, D.; Hobza, P. Electronic Structures, Vibrational Spectra, and Revised Assignment of Aniline and Its Radical Cation: Theoretical Study. *J. Chem. Phys.* **2003**, *118*, 10900−10911.
(57) Nibbering, E. T. J.; Elsaesser, T. Ultrafast Vibrational Dynamics of Hydrogen Bonds in the Condensed Phase. *Chem. Rev.* **2004**, *104*, 1887−1914.